Angewandte Chemie
Eine Zeitschrift der Gesellschaft Deutscher Chemiker

Supporting Information

Exfoliated 2D Layered and Nonlayered Metal Phosphorous Trichalcogenides Nanosheets as Promising Electrocatalysts for CO_2 Reduction

H. Wang, Y. Jiao, B. Wu, D. Wang, Y. Hu, F. Liang, C. Shen*, A. Knauer, D. Ren*, H. Wang*, P. A. van Aken, H. Zhang, Z. Sofer, M. Grätzel, P. Schaaf*

Experimental Procedures

Chemicals. Red phosphorus (99.999%), sulfur (99.999%), tin granules (99.999%) were obtained from STREM, Germany. Cobalt (99.9%), and nickel (99.9%) in powder form (−100 mesh) were obtained from Alfa Aesar, Germany. Isopropanol (IPA) (99%), acetone (99%), $KHCO_3$, and H_2SO_4 were purchased from Sigma-Aldrich. Deionized water (18.2 MΩ•cm) was made from Purelab Ultra. Carbon dioxide (CO_2, 99.998%) and Helium (He, 99.9999%) were purchased from Carbagas Company.

Characterization. The morphology of the prepared metal phosphorous trichalcogenides ($MPCh_3$) nanosheets was characterized using atomic force microscopy (AFM) equipped with a Dimension 3100 (Veeco, CA) in Height mode. Transmission electron microscopy (TEM) samples were prepared using the drop-casting method: a drop of sample dispersion was placed on a carbon-coated Cu grid and dried in air. Scanning transmission electron microscopy (STEM) investigations were carried out using a spherical aberration-corrected microscope (JEOL JEM-ARM 200F) with a DCOR probe corrector (CEOS GmbH) at 200 kV. high-angle anular dark-field STEM (HAADF-STEM) imaging was performed with a convergent semi-angle of 20.4 mrad and the collection semi-angle of 70-300 mrad. A collection semi-angle of 111 mrad was used for Electron energy-loss spectroscopy (EELS) measurements with a Gatan K2 Summit camera. EELS spectrum imaging was performed with a dispersion of 0.25 eV/channel with a 4000-pixel wide detector for the simultaneous acquisition of spectrum images of constituent elements. The raw spectrum image data were first denoised by applying the principal component analysis (PCA) with the multivariate statistical analysis (MSA) plugin (HREM Research Inc.) in Gatan DigitalMicrograph and then smoothed using a spatial filter in Gatan DigitalMicrograph. The Raman studies of the films were carried out on a WITec CRM200 confocal Raman microscopy system with a laser excitation energy of 532 nm and an air cooling charge-coupled device (CCD) as the detector. The scanning electron microscopy (SEM) images were obtained by Hitachi S-4800. The X-ray photoelectron spectroscopy (XPS) analysis was carried out using monochromatic Al_K-alpha radiation (excitation energy hv = 1,486.68 eV) using a SPECS SAGE HR 150 XPS system equipped with a 1D delayline detector and a Phoibos 150 analyzer. The calibration of the energy scale was ensured by reference measurements on a polycrystalline silver sample. 14 kV and an applied power of 300 W with samples mounted on indium foil. X-ray diffraction (XRD, SIEMENS/BRUKER D5000 and Bruker D8 ADVANCE, both with Cu anode) was used to measure the samples' crystalline structure. UV-Vis absorption spectra were measured from a Cary 5000 machine. The linear sweep voltammetry (LSV) was recorded with Gamry through a three-electrode system which was the same as the ECR system at a scan rate of 50 mV/s.

Synthesis of metal phosphorous trichalcogenides. A stoichiometric amount of metal, phosphorus, and sulfur corresponding to 15 g of thiophosphite was placed in a quartz glass ampule (30 × 150 mm; wall thickness 3 mm) and sealed under a high vacuum (below 1×10^{-3} Pa) using oxygen/hydrogen welding torch. The ampules ($NiPS_3$, $SnPS_3$) were placed in the muffle furnace and heated at 650 °C for 120 h and at 700°C each for 120 h. The heating rate was 1 °C/min, and the cooling rate was 1 °C/min. $CoPS_3$ was heated for 300 h at 550 °C (heating and cooling rate was 1 °C/min).

Preparation of $MPCh_3$ ultra-thin nanosheets. 0.5 g $MPCh_3$ powder and 1.5 mL IPA or acetone were added to a mortar and ground for 30 min. When the grinding solvent evaporates, an additional 1.5 mL was added to the mortar. The obtained sample (100 mg) was added to 10 mL IPA, and an ultrasonic bath (sonication frequency ~ 90 kHz) was used for continuous ultrasonic treatment for 2.0 h. Afterwards, the prepared dispersions were centrifuged at 250 g (Thermo Megafuge 16) for 30 minutes. After centrifugation, 3/4 of the supernatant was retained and subjected to a second centrifugation under the same conditions. Finally 2/3 of the obtained supernatant was retained for testing.

Preparation of cathode electrodes. Airbrushing method (VL-3AS, Paasche Airbrush Company) used to prepare the cathode electrode. The inks contained $MPCh_3$ dispersions, followed by 1 h ultrasonic dispersion. These inks were sprayed onto the hydrophobic side of the gas diffusion electrode (GDE, Sigracet 38 BC, FuelCellStore) using an airbrush set, followed by 12 h drying in the fume hood. The $MPCh_3$ electrodes were cut to slices of 2 cm × 2 cm before usage.

Preparation of anode electrode. The preparation of Pt (99.999%) anode with the thickness of 100 nm onto the GDE was used with the sputtering method (DP650, Concept Alliance). The Pt electrodes were cut to slices of 3 cm × 3 cm before usage.

Electrochemical CO_2 reduction. ECR was performed in a custom-built electrochemical flow cell,[1] including four chambers, i.e. the anode/cathode gas chambers and anode/cathode liquid chambers. The liquid chambers were made of PEEK material and separated by an anion exchange membrane (AMV, FumaTech Gmbh). The gas chambers were made of Stainless Steel. A KCl-saturated Ag/AgCl reference electrode (Pine Instruments) was immersed into the cathode liquid chamber. CO_2 gas (99.998%, Carbagas) and aqueous 0.5 M $KHCO_3$ electrolyte were infused into the gas chambers at a constant speed of 5 $cm^3\ min^{-1}$ (controlled by a mass flow controller, Alicat Scientific) and liquid chambers at a constant speed of 0.12 $cm^3\ min^{-1}$ (controlled by a peristaltic pump, IPC-4, Ismatec), respectively. The flow cell was connected to the potentiostat (Interface 1000, Gamry Instruments). The cathode gas chamber, the anode gas chamber and an Ag/AgCl electrode were connected to the working electrode (WE), counter electrode (CE) and reference electrode (RE), respectively. Anode gas chamber product and anode liquid chamber product were waste. For anodic reaction :

$$2H_2O \rightarrow O_2 + 4H^+ + 4e^- \qquad (1)$$

SUPPORTING INFORMATION

Products quantification. The gas products were analyzed by online gas chromatography (GC, Trace ULRTA, Thermo Fisher Scientific). The products were separated by a Shincarbon Column (Restek) and identified by a pulse discharge detector (PDD, Vici).

The liquid products were analyzed using high-performance liquid chromatography (HPLC, Agilent 1260). The solution consisted of 900 μL catholyte and 100 μL of 0.5 M H_2SO_4.

The faradaic efficiency (FE) and current density (*j*) of a specific product were defined as:

$$FE_X = \frac{Amount\ of\ electrons\ for\ producing\ X}{Total\ amount\ of\ electrons} \times 100\% \quad (2)$$

$$j_X = FE_X \times j_{total} \quad (3)$$

Computational details. The density functional theory (DFT) calculations were done using the Vienna *Ab-Initio* Simulation Package code.[2] The exchange correlation interactions and the ion–electron interactions were solved by the Perdew–Burke–Ernzerhof functionals and the projected-augmented wave method,[3] respectively. The $MPCh_3$ (X=Co, Ni, and Sn) monolayers were modelled using 2 × 2 supercells. A plane-wave cutoff of 450 eV was adopted and the maximal force on all-atom was below 0.02 eV/Å. The distance between periodic units in the direction perpendicular to the atomic sheets was larger than 16 Å. The chemical potential is considered to be equal to the free energy of the proton electron pair ($H^+ + e^+ \rightarrow 1/2\ H_2$). The ΔG value can then be determined as follows: ΔG = ΔE + ΔZPE −TΔS, where ΔE is the adsorption energy, ΔZPE is the change in zero-point energies, T is the temperature (T =298.15 K), and ΔS is the change of entropy. The adsorption energy ΔE is defined as: $\Delta E = E^*_{ads.} - (E^* + E_{ads.})$, where *ads. and * denote the adsorption of adsorbate on the substrates and bare substrates, $E_{ads.}$ denotes the energy of adsorbate. The zero-point energies and entropies of the CO_2 reduction species are determined from the vibrational frequencies in which only the adsorbed species' vibrational modes are computed explicitly with the substrates fixed. For HCOOH (aq):

$$CO_2 + 2(H^+ + e^-) + {}^* \rightarrow HCOO^* + H^+ + e^- \quad (4)$$

$$HCOO^* + H^+ + e^- \rightarrow {}^* + HCOOH \quad (5)$$

For CO (gas):

$$CO_2 + 2(H^+ + e^-) + {}^* \rightarrow HOOC^* + H^+ + e^- \quad (6)$$

$$HOOC^* + H^+ + e^- \rightarrow CO^* + H_2O \quad (7)$$

$$CO^* + H_2O \rightarrow {}^* + CO + H_2O \quad (8)$$

where * is the surface adsorption site.

SUPPORTING INFORMATION

Figures

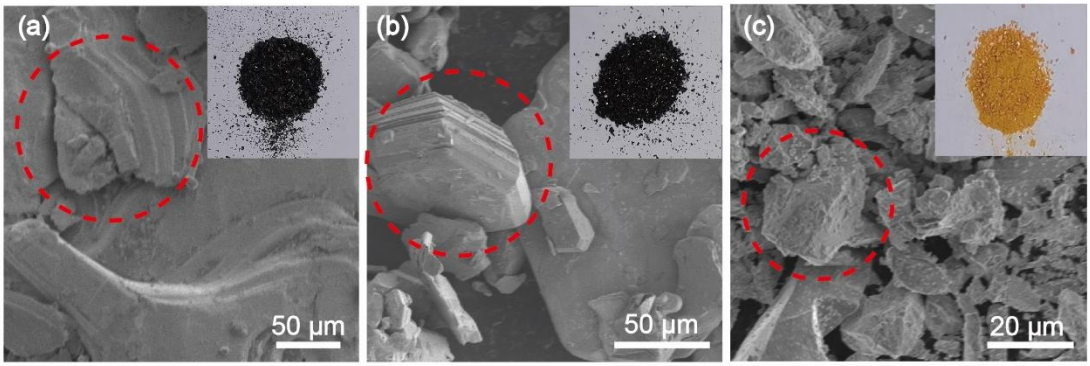

Figure S1. SEM images and photographs (inset) of the bulk $CoPS_3$ (a), bulk $NiPS_3$ (b), and bulk $SnPS_3$ (c) powders.

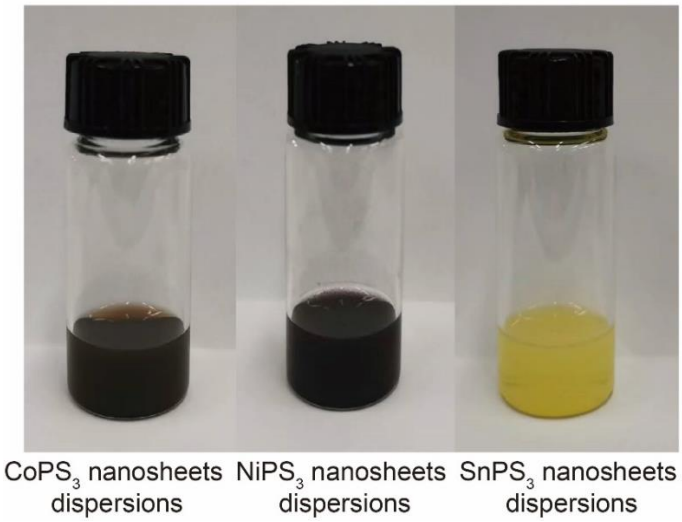

Figure S2. Photographs of the $MPCh_3$ nanosheets dispersions in IPA.

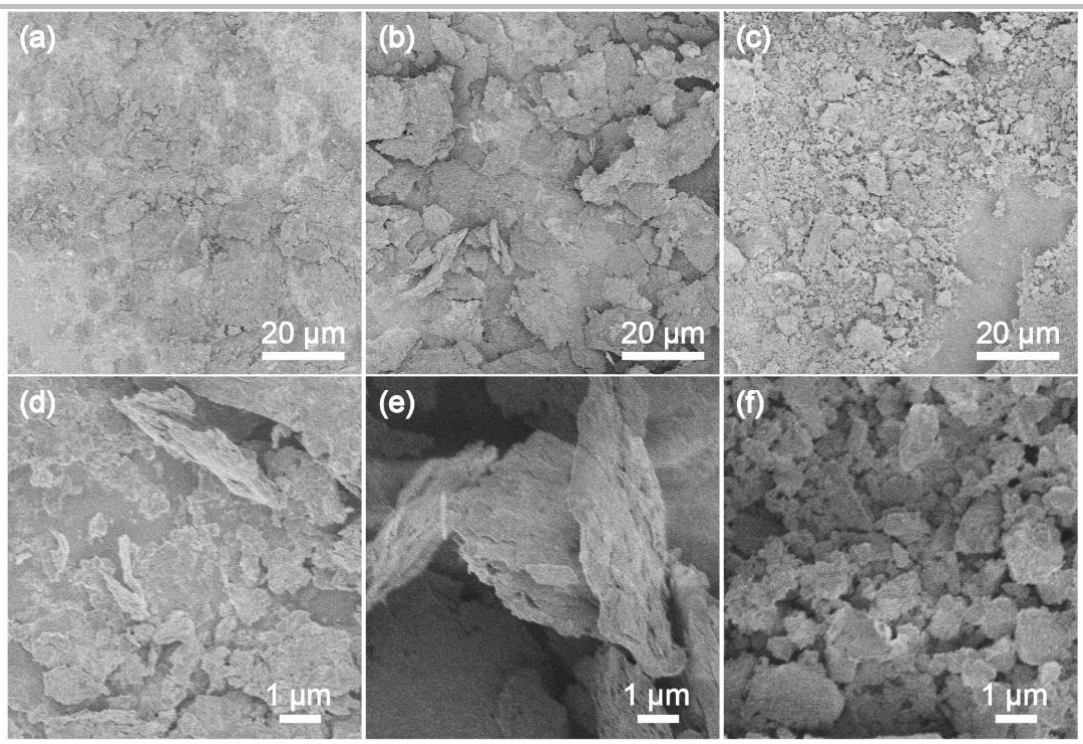

Figure S3. SEM images (a-c) and its corresponding enlarged SEM images (d-f) of the $CoPS_3$, $NiPS_3$, and $SnPS_3$ bulk crystals after grinding.

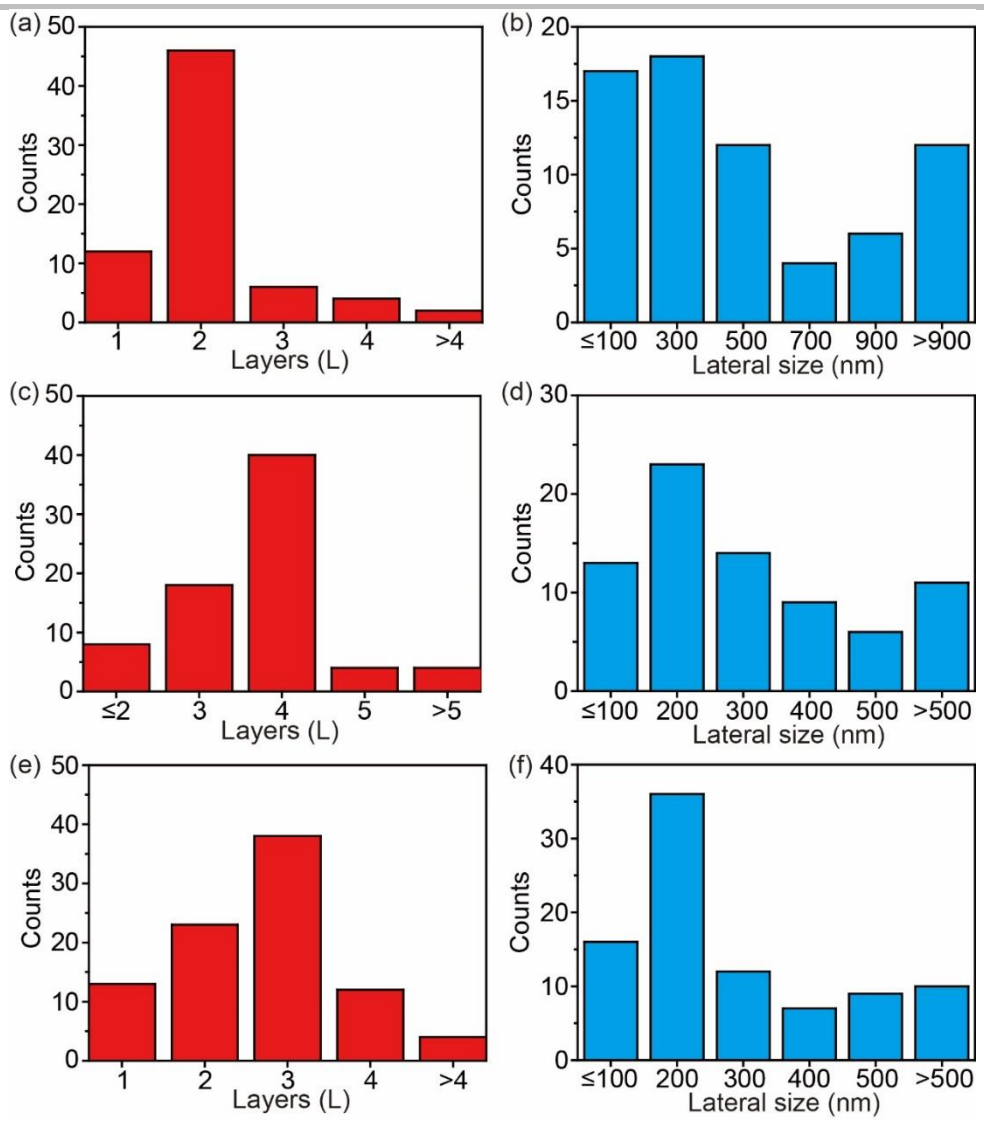

Figure S4. The corresponding thickness and lateral size distributions of the $CoPS_3$ nanosheets (a, b), $NiPS_3$ nanosheets (c, d), and $SnPS_3$ nanosheets (e, f) from the AFM images.

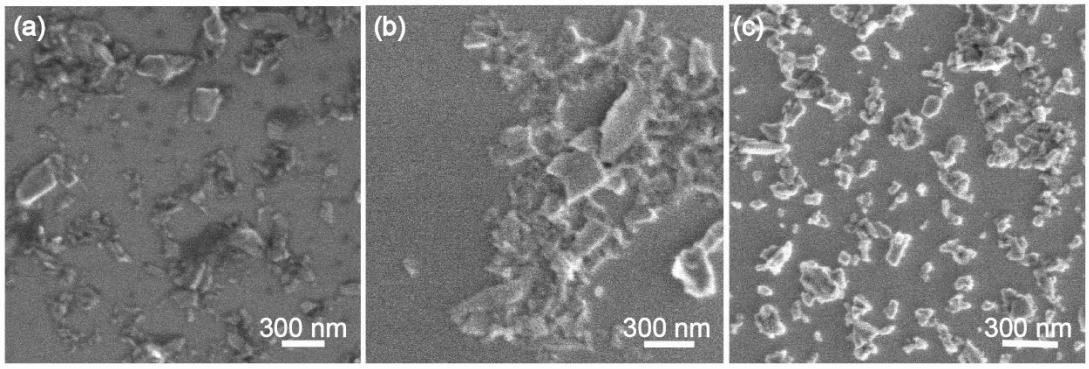

Figure S5. SEM images of $CoPS_3$ nanosheets (a), $NiPS_3$ nanosheets (b), and $SnPS_3$ nanosheets (c).

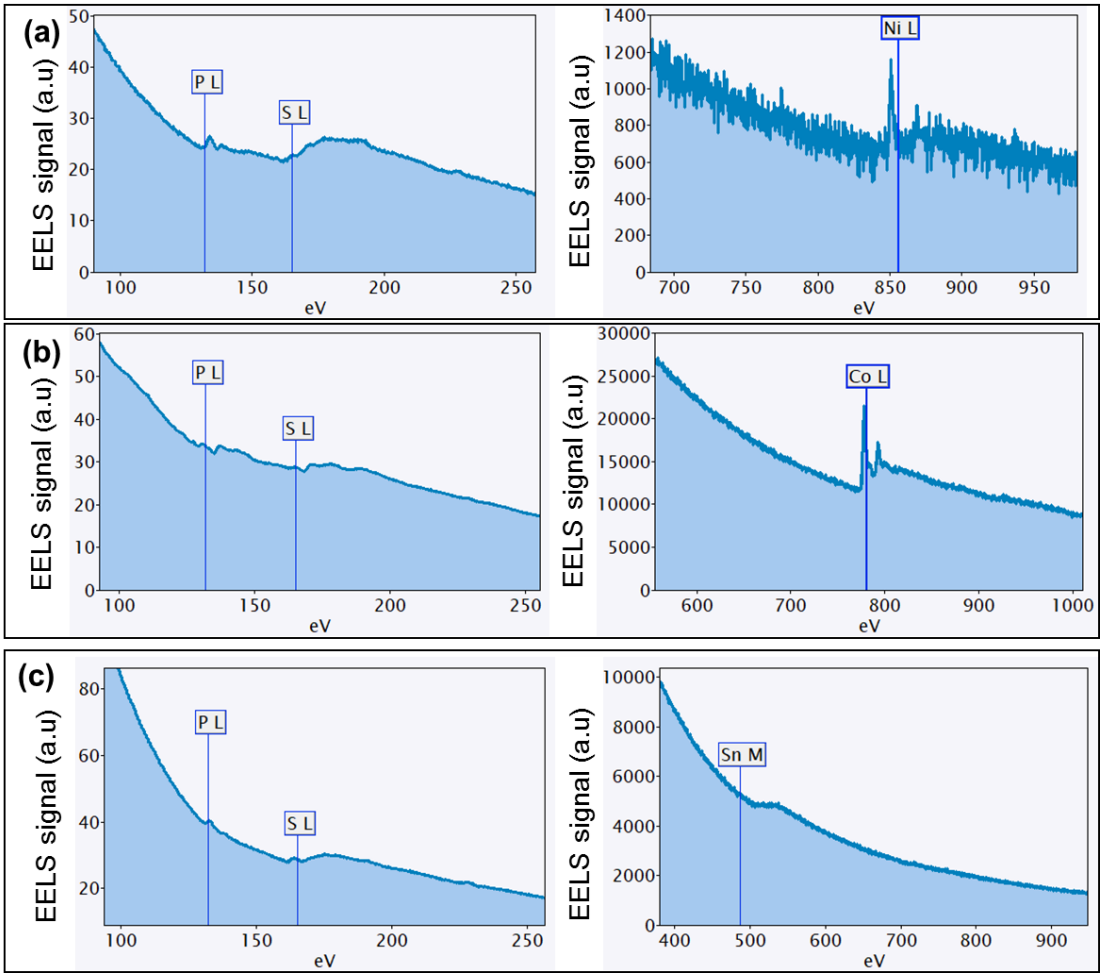

Figure S6. EELS spectrum of $NiPS_3$ (a), $CoPS_3$ (b) and $SnPS_3$ (c) nanosheets.

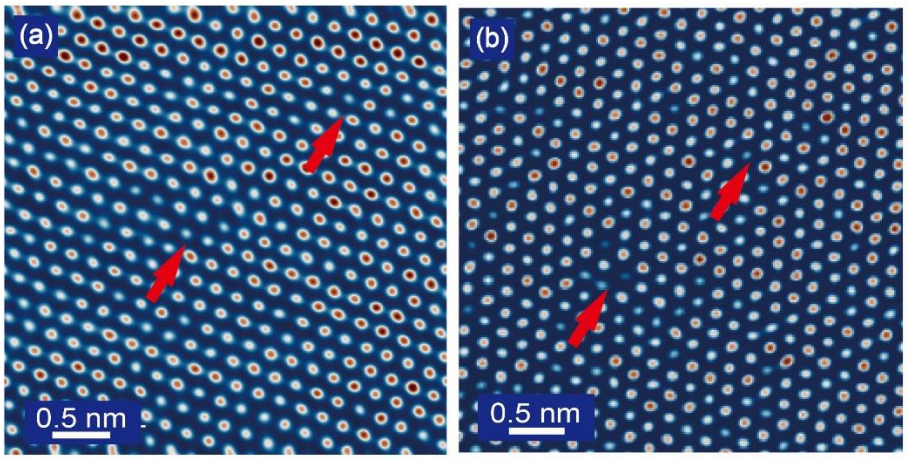

Figure S7. HAADF-STEM image of $CoPS_3$ and $NiPS_3$ nanosheets with point defects.

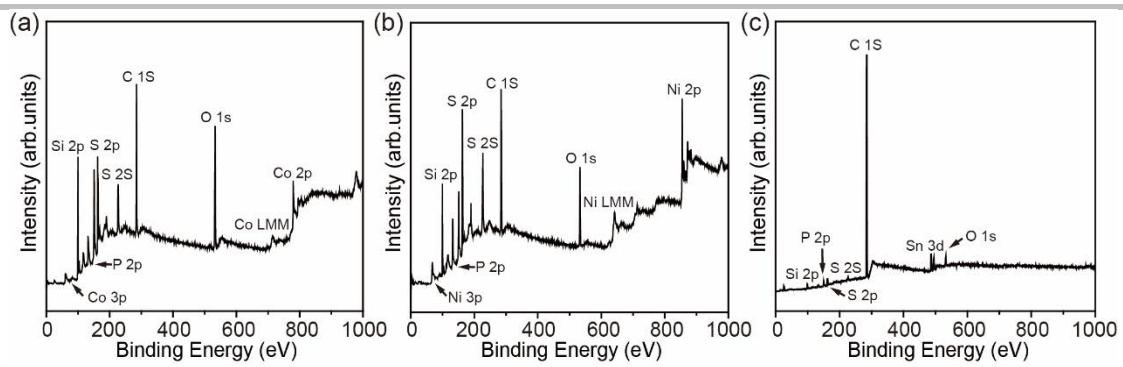

Figure S8. XPS survey spectra of $CoPS_3$ nanosheets (a), $NiPS_3$ nanosheets (b), and $SnPS_3$ nanosheets (c) deposited on a Si wafer.

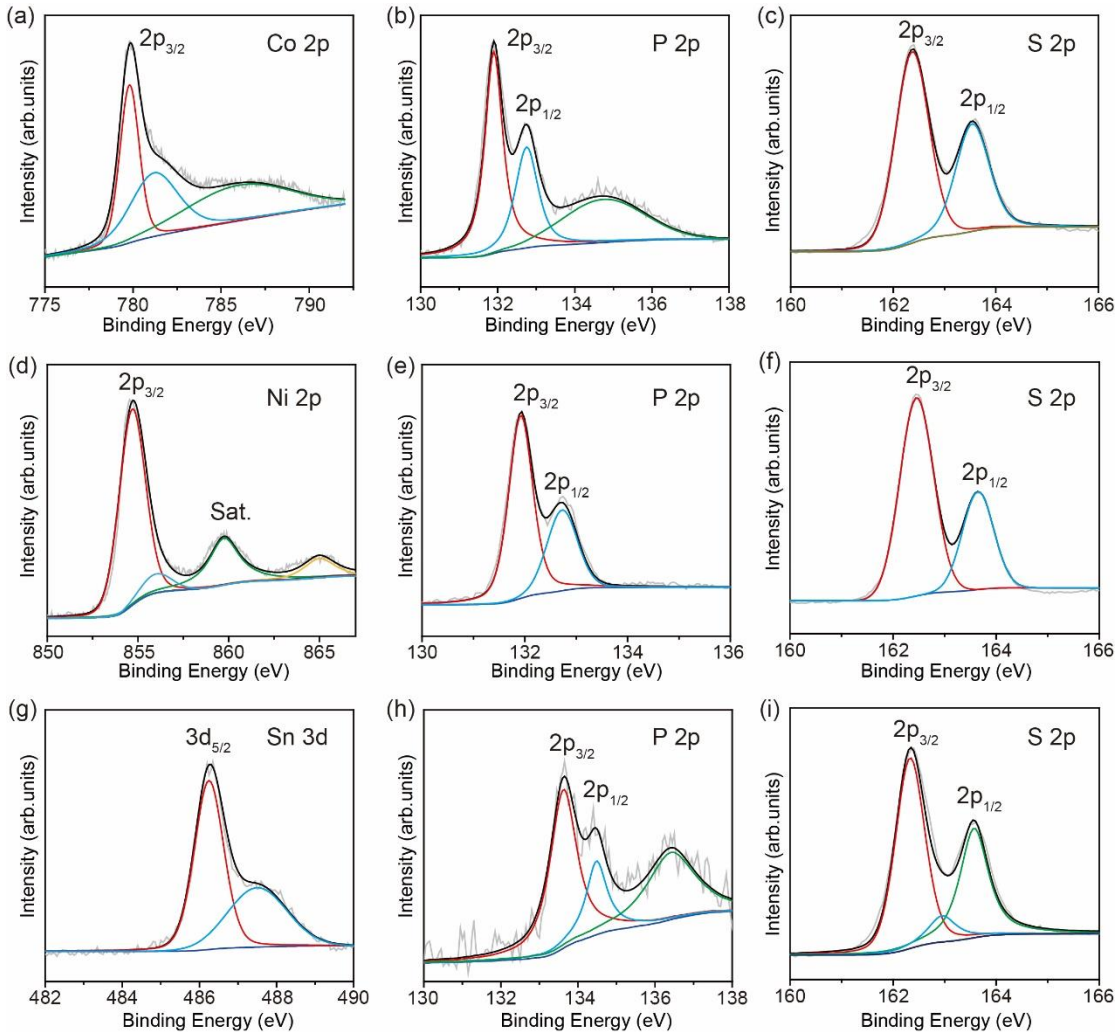

Figure S9. High resolution XPS spectra of the Co 2p (a), P 2p (b), and S 2p (c) states of $CoPS_3$ nanosheets. High resolution XPS spectra of the Ni 2p (d), P 2p (e), and S 2p (f) states of $NiPS_3$ nanosheets. High resolution XPS spectra of the Sn 3d (g), P 2p (h), S 2p (i) and states of $SnPS_3$ nanosheets.

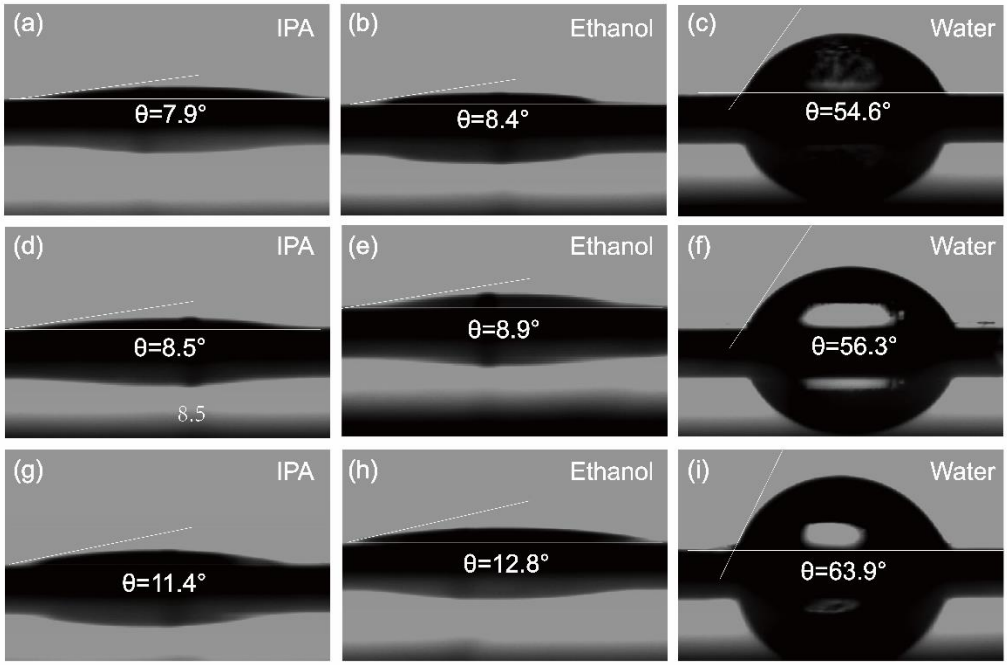

Figure S10. Photographs of static contact angles of $CoPS_3$ (a-c), $NiPS_3$ (d-f), and $SnPS_3$ (g-i) nanosheets and IPA (a, d, j), ethanol (b, e, g), and water (c, f, i).

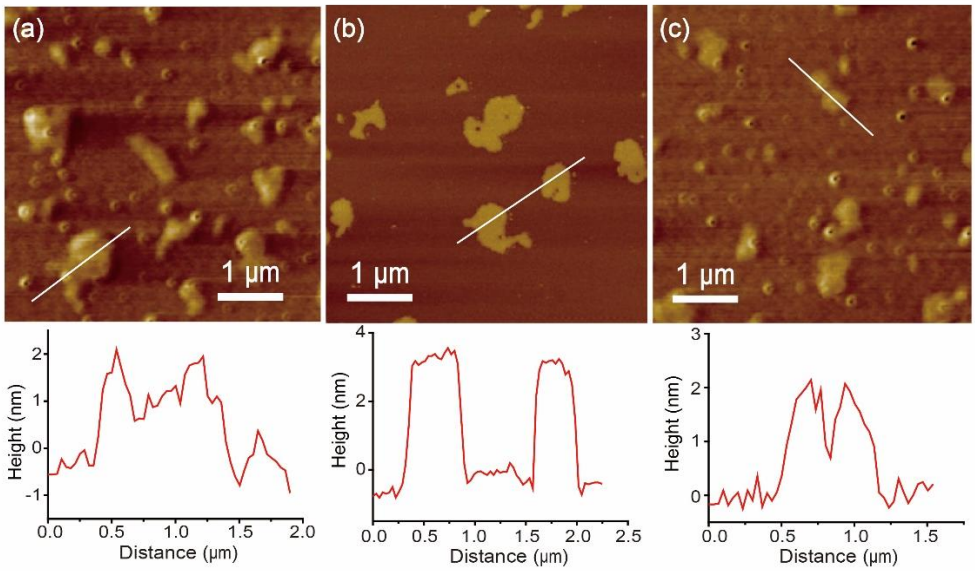

Figure S11. AFM images and the corresponding height profiles of exfoliated $CoPS_3$ nanosheets (c), $NiPS_3$ nanosheets (d), and $SnPS_3$ nanosheets (e) using acetone as grinding solvent.

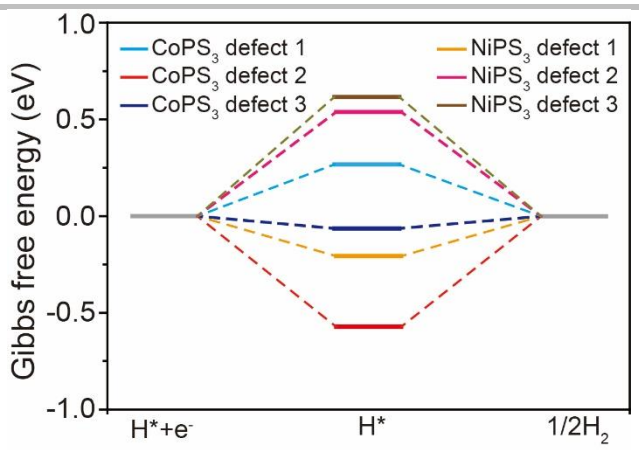

Figure S12. Calculated potential free energy diagrams for HER on the $CoPS_3$ and $NiPS_3$ surface of different defect concentrations. See information Figure S14 for the corresponding different defect concentrations.

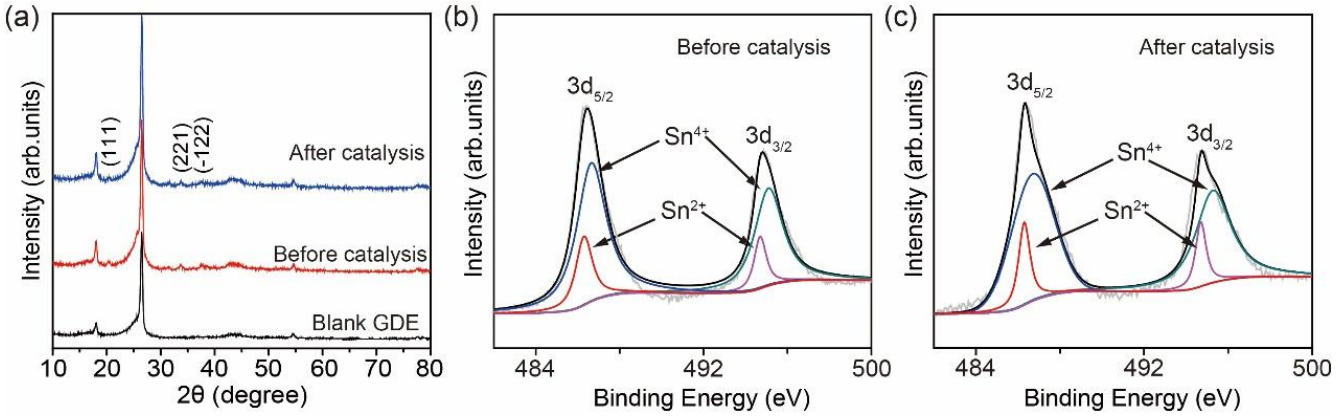

Figure S13. XRD pattern (a) and Sn 3d XPS spectra (b, c) of $SnPS_3$ catalysts deposited on GDE substrate before and after CO_2 ECR.

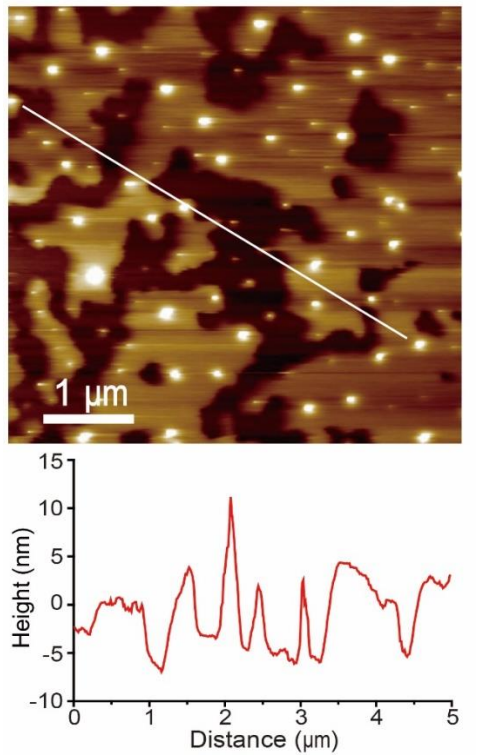

Figure S14. AFM image and the corresponding height profiles of exfoliated $SnPS_3$ nanosheets at lower centrifugal force (150 g) for 30 minutes.

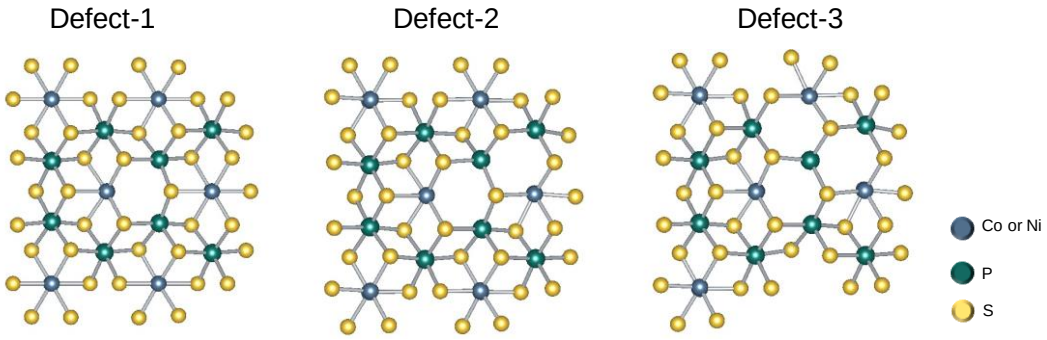

Figure S15. The structure geometries for different defect concentrations. For instance, defect-1 means introducing one sulfur vacancy surrounding the specific transition metal atom, and defect-2 and defect-3 mean two and three sulfur vacancies surrounding the transition metal atom, respectively.

SUPPORTING INFORMATION

Tables

Table S1. Summary of reported traditional exfoliation methods of $MPCh_3$ nanosheets in comparison to this work.

Materials	Grinding solvent	Grinding time	Sonicating solvent	Sonication time	Thickness of nanosheets	Reference
$NiPS_3$	_	_	Water	6 h	3.5 nm	[4]
$NiPS_3$	_	_	Ethanol	200 min	3.16 nm	[5]
$NiPS_3$	_	12 h	Ethanol	6 h	3.3-4.5 nm	[6]
$CoPS_3$	IPA/water	1 h	_	_	5.7-48 nm	[7]
$SnPS_3$	_	8 h	IPA	24 h	1.3-3.7 nm	[8]
$AgInP_2S_6$	_	_	Ethanol	12 h	0.7 nm	[9]
$Fe_2P_2S_6$	_	_	Acetone	4 h	1.3 nm	[10]
$NiPS_3$	IPA	30 min	IPA	2 h	2.0-3.5 nm	This Work
$CoPS_3$					0.7-1.5 nm	
$SnPS_3$					2.0 nm	

Table S2. Faradaic efficiency and current density of major products using $SnPS_3$ catalyst at different applied potentials.

Potential (V *vs.* RHE)	H_2 (%)	CO (%)	$HCOO^-$ (%)	Total (%)	j_{total} (mA cm^{-2})	j_{HCOO-} (mA cm^{-2})
-0.45	4.56	0.21	2.22	6.99	-10.39	-0.23
-0.55	37.70	5.10	25.80	68.6	-12.79	-3.30
-0.65	16.71	5.95	31.60	54.26	-23.76	-7.51
-0.75	15.70	0.20	22.50	38.4	-35.80	-8.06

Table S3. Faradaic efficiency and current density of major products using $CoPS_3$ catalyst at different applied potentials.

Potential (V *vs.* RHE)	H_2 (%)	CO (%)	CH_4 (%)	$HCOO^-$ (%)	Total (%)	j_{total} (mA cm^{-2})
-0.45	74.52			2.1	76.62	-23.78
-0.55	71.57	0.02		3.6	75.19	-24.26
-0.65	106.15	0.02	0.04	1	107.21	-143.32
-0.75	97.13	0.53	0.05	0.7	98.41	-224.58

Table S4. Faradaic efficiency and current density of major products using $NiPS_3$ catalyst at different applied potentials.

Potential (V *vs.* RHE)	H_2 (%)	CO (%)	Total (%)	j_{total} (mA cm^{-2})
-0.45	55.81	0.00	55.81	-11.03
-0.55	31.28	0.00	31.28	-15.52
-0.65	109.00	0.16	109.16	-18.06
-0.75	107.01	0.30	107.31	-23.21

Table S5. Faradaic efficiency and current density of major products using thick $SnPS_3$ catalyst at different applied potentials.

Potential (V *vs.* RHE)	H_2 (%)	CO (%)	$HCOO^-$ (%)	Total (%)	j_{total} (mA cm^{-2})	j_{HCOO-} (mA cm^{-2})
-0.45	37.17	0.29	0.49	37.95	-9.47	-0.05
-0.55	20.47	2.78	15.48	38.73	-11.18	-1.73
-0.65	13.20	1.61	22.30	37.11	-21.68	-4.83
-0.75	11.50	0.84	14.74	27.08	-48.28	-7.12

References

[1] D. Ren, J. Gao, L. Pan, Z. Wang, J. Luo, S. M. Zakeeruddin, A. Hagfeldt, M. Grätzel, *Angew. Chem. Int. Ed.* **2019**, *58*, 15036–15040.
[2] a) G. Kresse, J. Furthmüller, *Phys. Rev. B* **1996**, *54*, 11169; b) G. Kresse, D. Joubert, *Phys. Rev. B* **1999**, *59*, 1758.
[3] J. P. Perdew, A. Ruzsinszky, G. I. Csonka, O. A. Vydrov, G. E. Scuseria, L. A. Constantin, X. Zhou, K. Burke, *Phys. Rev. Lett.* **2008**, *100*, 136406.
[4] S. Xue, L. Chen, Z. Liu, H.-M. Cheng, W. Ren, *ACS Nano* **2018**, *12*, 5297–5305.
[5] J. Ran, H. Zhang, S. Fu, M. Jaroniec, J. Shan, B. Xia, Y. Qu, J. Qu, S. Chen, L. Song, J. M. Cairney, L. Jing, S-Z. Qiao, *Nat. Commun.* **2022**, *13*, 4600.
[6] Y. Tong, P. Chen, L. Chen, X. Cui, *ChemSusChem* **2021**, *14*, 2576-2584.
[7] F. M. Oliveira, J. Paštika, V. Mazánek, M. Melle-Franco, Z. Sofer, R. Gusmão, *ACS Appl. Mater. Interfaces* **2021**, *13*, 23638–23646.
[8] S. Huang, C. Meng, M. Xiao, S. Ren, S. Wang, D. Han, L. Sun, Y. Meng, *Nano Energy* **2019**, *61*, 462–470.
[9] W. Gao, S. Li, H. He, X. Li, Z. Cheng, Y. Yang, J. Wang, Q. Shen, X. Wang, Y. Xiong, Y. Zhou, Z. Zou, *Nat. Commun.* **2021**, *12*, 4747.
[10] L. Ji, L. Chang, Y. Zhang, S. Mou, T. Wang, Y. Luo, Z. Wang, X. Sun, *ACS Catal.* **2019**, *9*, 9721-9725.

Author contributions

H.W. led the project. H.W. and B.W. prepared the samples. H.W., Y.J., and C.S. wrote the manuscript. H.W., D.W., H.W., and P.S. designed and conceived this work. H.W., Y.J., B.W., Y.H., F.L., C.S., A.K., D.R., and H.W. contributed to measurements. D.W., C.S., D.R., H.W., P.A.v.A., H.Z., Z.S., M.G., and P.S. discussed some questions and modified the manuscript. P.S. guided this project. All authors discussed the results and commented on the manuscript.